Article

Inducing Spin Crossover in Metallo-supramolecular Polyelectrolytes through an Amphiphilic Phase Transition

Yves Bodenthin, Ullrich Pietsch, Helmuth Mhwald, and Dirk G. Kurth

J. Am. Chem. Soc., **2005**, 127 (9), 3110-3114• DOI: 10.1021/ja0447210 • Publication Date (Web): 10 February 2005

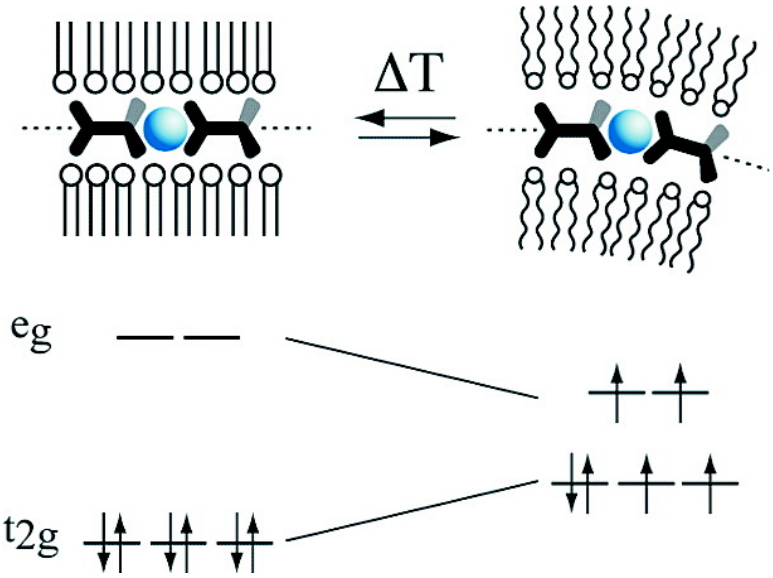

J|A|C|S
ARTICLES
Published on Web 02/10/2005

Inducing Spin Crossover in Metallo-supramolecular Polyelectrolytes through an Amphiphilic Phase Transition

Yves Bodenthin,[‡] Ullrich Pietsch,[‡] Helmuth Möhwald,[†] and Dirk G. Kurth*[,†,§]

Contribution from the Department of Physics, University of Potsdam, D-14424 Potsdam, Germany, Max Planck Institute of Colloids and Interfaces, D-14424 Potsdam, Germany, and National Institute for Materials Science, 1-1 Namiki, Tsukuba, Ibaraki 305-0044, Japan

Received September 1, 2004; E-mail: kurth@mpikg-golm.mpg.de

Abstract: A phase transition in an amphiphilic mesophase is explored to deliberately induce mechanical strain in an assembly of tightly coupled metal ion coordination centers. Melting of the alkyl chains in the amphiphilic mesophase causes distortion of the coordination geometry around the central transition metal ion. As a result, the crystal field splitting of the d-orbital subsets decreases resulting in a spin transition from a low-spin to a high-spin state. The diamagnetic−paramagnetic transition is reversible. This concept is demonstrated in a metallo-supramolecular coordination polyelectrolyte−amphiphile complex self-assembled from ditopic bis-terpyridines, Fe(II) as central transition metal, and dialkyl phosphates as amphiphiles. The magnetic properties are studied in a Langmuir−Blodgett multilayer. The modularity of this concept provides extensive control of structure and function from molecular to macroscopic length scales and gives access to a wide range of new molecular magnetic architectures such as nanostructures, thin films, and liquid crystals.

Metallo-supramolecular modules (MEMOs) are at the focus of materials research for the construction of functional devices for recognition (sensing), transformation (catalysis), and translocation (signal transduction).[1] The increasing importance of MEMOs rests on the fact that assembly of metal ions and ligands provides an elegant and efficient access to a plethora of well-defined structures and value-adding functions.[2] The occurrence of semi-occupied d-orbitals gives rise to some of the most prominent properties of MEMOs, including strong absorption, high quantum yields, suitable excited-state lifetimes, luminescence, and tunable redox states. The splitting of the d-orbitals in a ligand field of appropriate symmetry and strength can give rise to thermally induced or photoinduced spin transition and spin crossover phenomena, the most intriguing one being light-induced excited spin state trapping (LIESST),[3] reverse[4] and low-spin LIESST,[5] but also metal-to-ligand charge transfer in nitroprusside,[6] metal-to-metal charge transfer as in prussian blue analogues,[7] and valence tautomerism,[8] as well as ligand-driven light-induced spin-state change (LD-LISC).[9]

The conversion between a low-spin (LS) and high-spin (HS) state is typically observed in transition metal ion compounds with a $3d^n$ ($4 \leq n \leq 7$) electronic configuration, the most extensively studied element being the Fe(II) ion. In a ligand field of octahedral symmetry, the d-orbitals split in low-lying t_{2g} and high-lying e_g subsets. In the case of the Fe(II) ion, the LS state arises from a closed-shell t_{2g}^6 electronic configuration and the HS state from a $t_{2g}^4e_g^2$ electronic configuration, respectively. The spin crossover is generally accompanied by a change in the optical and magnetic properties, as well as a lengthening of the metal ion−ligand bond due to the occupation of the anti-bonding e_g subset.[10] Generally, thermal spin crossover is a molecular process, driven by the entropy gain on going from the LS to the HS state.[11] Spin transitions occur in liquids, liquid crystals, and solids.[12]

Two principal strategies have been adopted in ligand design in order to affect the spin state of the coordinating metal ion. The strength of the ligand field can be reduced by either steric strain or steric bulk in the coordinating ligands, thus making the HS configuration more favorable.[13] For instance, 2,2′:6′,2″-

[‡] University of Potsdam.
[†] Max Planck Institute of Colloids and Interfaces.
[§] National Institute for Materials Science, Japan.

(1) Lehn, J.-M. *Supramolecular Chemistry: Concepts and Perspectives*; VCH: Weinheim, Germany, 1995. Lehn, J.-M. *Science* **2002**, *295*, 2400. Lehn, J.-M. *Proc. Natl. Acad. Sci. U.S.A.* **2002**, *99*, 4763−4768. Whitesides, G. M.; Grzybowski, B. *Science* **2002**, *295*, 2418.
(2) Holliday, B. J.; Mirkin, C. A. *Angew. Chem.* **2001**, *113*, 2076−2098.
(3) Decurtins, S.; Gütlich, P.; Kohler, C. P.; Spiering, H.; Hauser, A. *Chem. Phys. Lett.* **1984**, *105*, 1.
(4) Decurtins, S.; Gütlich, P.; Hasselbach, K. M.; Hauser, A.; Spiering, H. *Inorg. Chem.* **1985**, *24*, 2174.
(5) Renz, F.; Oshio, H.; Ksenofontov, V.; Waldeck, M.; Spiering, H.; Gütlich, P. *Angew. Chem., Int. Ed.* **2000**, *39*, 3699.
(6) Gu, Z. Z.; Sato, O.; Iyoda, T.; Hashimoto, K.; Fujishima, A. *J. Phys. Chem.* **1996**, *100*, 18289.
(7) Sato, O.; Iyota, A.; Fujishima, A.; Hashimoto, K. *Science* **1996**, *272*, 704.
(8) Attia, A. S.; Jung, O. S.; Pierpont, C. G. *Inorg. Chim. Acta* **1994**, *226*, 91.
(9) Boillot, M.-L.; Roux, C.; Audiere, J.-P.; Dausse, A.; Zarembowitch, J. *Inorg. Chem.* **1996**, *35*, 3975.
(10) Kahn, O.; Martinez, C. J. *Science* **1998**, *279*, 44.
(11) Gütlich, P.; Garcia, Y.; van Koningsbruggen, P. J.; Renz, F. Photo-Magnetism of Transition Metal Compounds. In *Introduction to Physical Techniques in Molecular Magnetism: Structrural and Macroscopic Techniques*; Palacio, F., Ressouche, E., Schweizer, J., Eds.; University Press: Zaragoza, Spanien, 2001.
(12) Galyametdinov, Y.; Ksenofontov, V.; Prosvirin, A.; Ovchinnikov, I.; Ivanova, G.; Gütlich, P.; Haase, W. *Angew. Chem., Int. Ed.* **2001**, *40*, 4269. Soyer, H.; Dupart, E.; Gómez-García, C. J.; Mingotaud, C.; Delhaès, P. *Adv. Mater.* **1999**, *11*, 382.

10.1021/ja0447210 CCC: $30.25

terpyridine (tpy) induces a strong ligand field; therefore, the resulting complexes with iron(II) of the form $[Fe(tpy)_2]X_2$ are exclusively LS, irrespectively of the counterion X. While substitution in the 4′-position of the central pyridine ring has no effect, it has recently been recognized that bulky substitutents in the 6- and/or 6″-position do affect the spin sate. Here, we report another approach to affect spin crossover by introducing mechanical strain through an amphiphilic phase transition in a lamellar superstructure containing a quasi one-dimensional rigid-rod-type metallo-supramolecular polyelectrolyte (MEPE) based on the ditopic bis-terpyridine 1,4-bis(2,2′:6′,2″-terpyridine-4′-yl)benzene, **3**.

Self-assembly of the ditopic bis-terpyridine ligand, **3**, and iron acetate in aqueous solution results in formation of MEPE, **2**.[14] Subsequent self-assembly of MEPE and dihexadecyl phosphate (DHP) affords the polyelectrolyte−amphiphile complex (PAC), **1**, as shown in Scheme 1.[15] Under the particular assembly conditions, the composition amounts to six DHPs per monomer unit $[Fe\mathbf{3}]^{2+}$. Presumably, DHP forms a charged hydrogen-bonded network which binds to MEPE through electrostatic interactions. The volume material as well as LB multilayer shows thermotropic polymorphism.[16] The hydrophobic character permits spreading PAC at the air−water interface.[17] The resulting Langmuir monolayer can be transferred on solid supports by means of the Langmuir−Blodgett (LB) technique.

Scheme 1 [a]

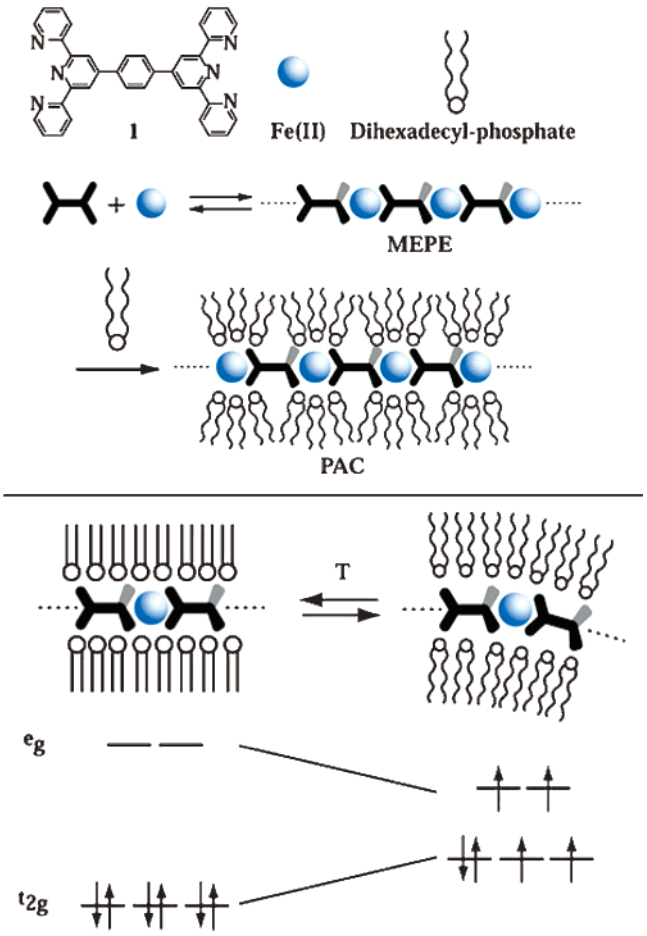

[a] (Top) Self-assembly of ditopic ligand **1** and $Fe(OAc)_2$ results in formation of the linear, rigid-rod-type metallo-supramolecular polyelectrolyte (MEPE). In a consecutive step, MEPE is assembled with dihexadecyl phosphate, resulting in formation of the corresponding polyelectrolyte−amphiphile complex (PAC). Spreading PAC at the air−water interface and subsequent transfer of the Langmuir monolayers on a solid support results in a well-defined multilayer, a section of which is schematically shown in the bottom of the scheme. (Bottom) Upon heating of the multilayer, the alkyl chains of the mesophase melt, resulting in a distortion of the metal ion coordination geometry. The unfavorable coordination of the terpyridines around the Fe(II) cation results in a lowering of the energy gap between the d-orbital subset, giving rise to a reversible transition from a diamagnetic low-spin state to a paramagnetic high-spin state.

Experimental Section

The LB transfer was carried out with a NIMA film balance (Hellma Optik, Forest Hills, NY). We used silicon wafers (Wacker AG, Munich) as substrates, which were cleaned according to the Kern procedure.[18] Monolayer transfer was carried out at 20 °C, at a constant surface pressure of 40 mN/m and a dipping speed of 6 mm/min. The transfer ratios were always 0.95 ± 0.05 for up- and downstroke deposition. X-ray reflectivity measurements were performed on a $\theta-2\theta$ diffractometer (Stoe & Cie) using Cu Kα radiation with a wavelength of $\lambda =$ 0.154 nm. The calculation of the reflectivity was performed using the Parrat formalism.[19] Grazing incidence diffraction measurements were carried out at the D4 beam line at the Hasylab synchrotron light source using an angular dispersive triple-axis diffractometer and a wavelength of $\lambda = 0.124$ nm. Temperature-dependent specular reflection and gracing incidence diffraction measurements were carried out at the Energy Dispersive Reflectometer at the BESSY II synchrotron light source using the experimental setup described in ref 24. Reflectance and diffraction data of a film were recorded at the given temperature using two energy-dispersive detectors. First, the reflectance data were recorded at an angle of incidence of 1°, after which the angle of incidence was changed to 0.2° to collect the diffraction data. All other experimental parameters were kept constant. Therefore, reflectance and diffraction experiments probed the same structure of the film at that temperature. The recording time for each spectrum was 60 s. Extended X-ray absorption fine structure (EXAFS) experiments were undertaken at the KMC 2 beam line at BESSY II, using the fluorescence yield $I_{fluo}(E) \sim \mu(E)$ of the Fe^{2+} ions, where $\mu(E)$ represents the absorption.[20] To increase the signal we used gracing incidence conditions ($\alpha_i =$ 0.15°−0.2°). The detector was attached perpendicular to the sample surface. To explore the data we used a simplex fitting algorithm minimizing the residual $S = [\sum(\chi_{exp}(k) - \chi_{sim}(k))^2/\sum\chi_{exp}^2(k)]^{0.5}$. χ_{sim} was calculated using the standard EXAFS formula $\chi_{sim} = \sum_i(N_i/kr_i^2)$ $\exp(-2\sigma_i^2k^2)$ $\exp[-2r_i/\lambda(k)]$ $|f_i(k,r_i)|$ $\sin[2kR_i + \Phi(k,r_i)]$, where k represents the reduced wavenumber $k = \hbar^{-1}[2m_e(E - E_0)]^{0.5}$, E the photon energy, E_0 the iron absorption edge, N_i the occupation number, σ^2 the Debye−Waller factor, and r_i the radius of the shell. The amplitude $f(k,r)$ and phase $\Phi(k,r)$ were calculated with the ab initio FEFF6 calculation. χ_{exp} is defined as $\chi_{exp}(k) = (\mu(k) - \mu_0(k))/\mu_0(k)$ and $\mu_0(k)$

(13) Constable, E. C.; Baum, G.; Bill, E.; Dyson, R.; van Eldik, R.; Fenske, D.; Kaderli, S.; Morris, D.; Neubrand, A.; Neuburger, M.; Smith, D. R.; Wieghardt, K.; Zehnder, M.; Zuberbuhler, A. D. *Chem. Eur. J.* **1999**, *5*, 498−508.
(14) Schütte, M.; Kurth, D. G.; Linford, M. R.; Cölfen, H.; Möhwald, H. *Angew. Chem.* **1998**, *110*, 3058−3061; *Angew. Chem., Int. Ed.* **1998**, *37*, 2891−2893.
(15) Kurth, D. G.; Lehmann, P.; Schütte, M. *Proc. Natl. Acad. Sci. U.S.A.* **2000**, *97*, 5704−5707.
(16) Kurth, D. G.; Meister, A.; Thünemann, A. F.; Förster, G. *Langmuir* **2003**, *19*, 4055.
(17) Lehmann, P.; Kurth, D. G.; Brezesinski, G.; Symietz, C. *Chem. Eur. J.* **2001**, *7*, 1646−1651.
(18) Kern, W. *Semicond. Int.* **1984**, 94.
(19) Parrat, L. G. *Phys. Rev.* **1954**, *95*, 359.
(20) Erko, A.; Packe, I.; Gudat, W.; Abrosimov, N.; Firsov, A. *Proc. SPIE−Int. Soc. Opt. Eng.* **2000**, *4145*, 122−128.
(21) Michalowicz, A.; Vlaic, G. *J. Synchrotron Radiat.* **1998**, *5*, 1317−1320.
(22) Kharchenko, A.; Englisch, U.; Geue, Th.; Grenzer, J.; Pietsch, U.; Siebrecht, R. *Neutron News* **2000**, *11*, 4.
(23) Bodenthin, Y.; Pietsch, U. *Bessy Annu. Rep.* **2001**, 239.
(24) Bodenthin, Y.; Grenzer, J.; Lauter, R.; Pietsch, U.; Lehmann, P.; Kurth, D. G.; Möhwald, H. *J. Synchrotron Radiat.* **2002**, *9*, 206−209. Bodenthin, Y.; Pietsch, U.; Grenzer, J.; Gene, Th.; Möhwald, H.; Kurth, D. G. *J. Phys. Chem. B*, in press.

represents the iron K absorption edge. To avoid the "multiple solution trap",[21] the Fe−N distances were restrained to vary in an interval of ±0.02 nm. The shift of the energy threshold, ΔE_0, remains constant at $\Delta E_0 = -4.3$ eV for all fits. Magnetic measurements were performed with a superconducting quantum interference device (SQUID) from Quantum Design with a sensitivity of $\leq 10^{-7}$ emu and an applied field of 10 kOe. The samples were aligned with the surface parallel to the applied magnetic field. Spin-resolved neutron reflectivity experiments were carried out at the ADAM reflectometer at the Institute Laue Langevin in Grenoble, France. The working wavelengths $\lambda = 0.44$ nm was selected from a white neutron beam by a graphite monochromator providing a flux of 2.6×10^6 s^{-1} cm^{-2}. The resolution is $\Delta\lambda/\lambda = 0.006$, and the background noise was about 10^{-5} counts/s (negligible).[22] The magnetic field was applied by an electromagnet attached parallel to the sample surface and parallel (or antiparallel) to the spin polarization direction. The vertical momentum transfer for both neutron and X-ray reflectometry is defined as $q_z = 2\pi/\lambda \sin 2\alpha_i$, where α_i describes the angle of incidence between the incoming beam and the sample surface. X-ray magnetic circular dichroism (XMCD) measurements at the iron L absorption edges (706 and 718 eV) were carried out at the UE 56/2 soft X-ray beamlines at BESSY II. We used a reflectivity setup where the samples were attached on a diffractometer stored in a vacuum chamber. The resonantly enhanced transition probability at absorption edges leads to larger dichroic effects compared to transmission geometries.[31] The vacuum stability of the samples was proved up to pressures of $p = 10^{-8}$ mPa. No structural changes appeared after transfer of the sample into the experimental chamber.[23] A magnetic field of about 3000 Oe, induced by permanent magnets below the sample, was applied parallel to the sample surface and parallel to the plane of incidence.

Results and Discussion

The architecture of the LB films is investigated by energy-dispersive X-ray reflectivity (XRR) and in-plane diffraction.[24] The XRR data of LB films measured at room temperature reveals Kiessig fringes as well as Bragg peaks, confirming the strict stratification of the supramolecular units with an interlayer lattice spacing of 5.7 ± 0.2 nm. Compared to the length of DHP (2.4 nm), this spacing corresponds to the head-to-head or tail-to-tail arrangement, respectively, of two adjacent PAC strata (Y-type arrangement). In addition, a distinct in-plane ordering is observed, characterized by a single in-plane Bragg peak with a lattice parameter of 0.42 ± 0.05 nm. This peak is consistent with a hexagonal packing of the alkyl chains. Upon heating, both the in-plane and out-of-plane signals vanish and decrease, respectively, indicating that the alkyl chains and the interlayer arrangement become disordered. Upon cooling of the sample, the in-plane Bragg peak and Kiessig fringes are recovered, indicating the reversibility of the phase transition.

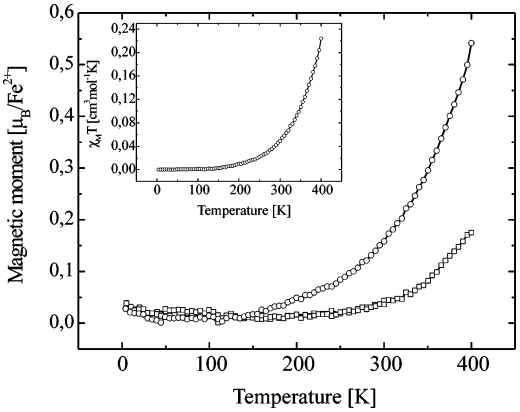

Figure 1. Temperature-dependent superconducting quantum interference device (SQUID) measurements of the magnetic moment for two samples consisting of 11 and 15 Langmuir monolayers in the temperature range from 5 to 400 K and $H = 10$ kOe. The material behaves diamagnetically at low temperatures and becomes paramagnetic above room temperature. We note that even at 400 K we do not observe saturation of the paramagnetic signal. (Inset) Measurement of the molar susceptibility as $\chi_M T$ vs T.

To determine the structure of the coordination sphere of the metallo units, we perform EXAFS at the iron Kα absorption edge ($E = 7.1$ keV).[25] Although the amount of Fe(II) in the sample is small, the corresponding EXAFS signal is strong enough to extract the next neighbor coordination sphere around the metal center. We note that the room-temperature spectra can only be simulated with a two-shell model assuming two different Fe−N bond distances, $R_1 = 0.182 \pm 1 \times 10^{-3}$ nm and $R_2 = 0.199 \pm 1 \times 10^{-3}$ nm, and occupation numbers of 2 and 4, respectively. These values correspond to a distorted octahedral coordination geometry with two N-atoms being in the central and four being in the terminal positions of the octahedron. These determined bond distances are in good agreement with data from single-crystal structure analysis of bis-terpy iron(II) complexes.[26]

Temperature-dependent EXAFS measurements indicate a structural change in the coordination geometry. In terms of the two-shell model, the data can be interpreted either by a regular increase of the octahedron by 2% or by a uniaxial elongation of the long axis by 4% for increasing temperature up to 348 K. We note that the Debye−Waller factor (Fe−N bonds) remains constant throughout the observed temperature range, which is in contrast to other thermally driven spin transition complexes.[27] Considering all the data, a temperature rise results in structural changes at all length scales. A change in the coordination geometry, that is, the bond length, as indicated by EXAFS is expected to affect the crystal field splitting. In particular, a lengthening of the Fe−N bond length is expected to reduce the splitting of the d-orbital subsets, thus opening the way for spin transitions in the material.

To verify this hypothesis, we determined the magnetic moments of the sample using SQUID in the temperature range from 5 to 400 K. Figure 1 shows the temperature-dependent magnetic moment for two samples consisting of 11 and 15 Langmuir monolayers deposited on silicon wafers. Whereas the material behaves diamagnetically at low temperatures, we observe an increasing paramagnetic signal above room temperature. The curves for heating and cooling are indistinguishable; that is, there is no hysteresis. The samples behave reversibly as two consecutive cycles are identical. We note that, even at

(25) Als-Nielsen, J.; McMorrow, D. *Elements of Modern X-ray Physics*; John Wiley and Sons Ltd.: New York, 2001.
(26) The average bond length in bis-terpyridine complexes of Fe(II) is 1.89 Å for the central and 1.98 Å for the terminal positions or 1.94 Å on average. See: (a) Baker, A. T.; Goodwin, H. A. *Aust. J. Chem.* **1985**, *38*, 207. (b) Laine, P.; Gourdon, A.; Launay, J.-P. *Inorg.Chem.* **1995**, *34*, 5156. (c) Constable, E. C.; Davies, J. E.; Phillips, D.; Raithby, P. R. *Polyhedron* **1998**, *17*, 3989.
(27) Yokoyama, T.; Murakami, Y.; Kiguchi, M.; Komatsu, T.; Kojima, N.; *Phys. Rev. B* **1998**, *58*, 14238. Michailowicz, A.; Moscovici, J.; Charton, J.; Sandid, F.; Benamrane, F.; Garcia, Y. *J. Synchrotron Radiat.* **2001**, *8*, 701.
(28) Siebrecht, R.; Schreyer, A.; Englisch, U.; Pietsch, U.; Zabel, H. *Physica B* **1998**, *241−243*, 169−171.
(29) Zabel, H.; Siebrecht, R.; Schreyer, A. *Physica B* **2000**, *276−278*, 17−21. Kharchenko, A.; Englisch, U.; Geue, T.; Grenzer, J.; Pietsch, U.; Siebrecht, R. *Neutron News* **2000**, *11*, 29−32.
(30) Chen, C. T.; Idzerda, Y. U.; Lin, H.-J.; Smith, N. V.; Meigs, G.; Chaban, E.; Ho, G. H.; Pellegrin, E.; Sette, F. *Phys. Rev. Lett.* **1995**, *75*, 152.
(31) Mertins, H.-Ch.; Abrahamsohn, D.; Gaupp, A.; Schäfers, F.; Gudat, W.; Zaharko, O.; Grimmer, H.; Oppeneer, P. M. *Phys. Rev. B* **2002**, *66*, 184404.

temperatures of 400 K, we do not observe saturation of the paramagnetic signal.

Spin-resolved neutron reflectivity (SNR) measurements are used to probe the magnetic moment of Fe(II) centers at room temperature.[28] Here, the direction of the magnetic moment of the sample is oriented perpendicular to the scattering plane using an external magnetic field of 7000 Oe. The scattering plane is defined by the vectors of the incident and reflected waves. The first-order Bragg peak appears at $q_z = 1.1$ nm^{-1} and is caused by both the core and magnetic scattering of the atoms. If we assume that the spin of the neutron remains unchanged after interaction with the sample, that is, a non-spin flip analysis, the scattering intensity is proportional to the scattering length $b = b_{nuc} \pm b_{mag} \sin \Theta$, where b_{nuc} is the scattering length of the nucleus, b_{mag} the magnetic scattering length, and Θ the angle between the magnetic moment of the sample, μ_s, and the scattering plane. The quantity b_{nuc} is independent of the scattering angle and the magnetic moment, μ_n, of the neutron. Through the external field, the magnetic moment of the sample, μ_s, is oriented parallel (spin-up) or antiparallel (spin-down) to the moment of the neutron, μ_n ($\sin \Theta = 1$). As indicated by the equation above, the scattering intensity depends on the orientation of the magnetic moment of the sample with respect to the spin polarization of the probing neutrons.[29] For the present supramolecular structure, we determine a difference in reflected intensities of the first Bragg peak for spin-up and spin-down neutrons of approximately 2% at room temperature. Simulation of the reflectivity data gives the magnetic scattering length, b_{mag}, which corresponds to a magnetic moment of $0.6 \pm 0.3\ \mu_B$ per iron ion, where μ_B is the Bohr magneton. In comparison, Constable reported a value of $5.3\ \mu_B$ over the temperature range from 290 to 40 K.[13] We assume that the experimentally determined value represents a lower limit, and since saturation has not been reached (vide supra), the magnetic moment should increase with temperature as more and more Fe(II) centers become distorted. Measurements at higher temperature are not possible with this method due to the decreasing intensity of structural Bragg peaks above the phase transition temperature.

Independently, we determined the magnetic moment by X-ray magnetic circular dichroism (XMCD),[30] which offers higher accuracy even for thin-film materials as compared to SNR. Here, the X-ray reflectivity of the multilayer is measured at a fixed angle of incidence ($\alpha_i = 2°$) using left- and right-handed circular polarized synchrotron radiation at room temperature (308 K) (see Figure 2). Due to the E^{-2} dependence of the reflectivity coefficient, the overall reflectivity decreases as a function of energy E of the probe beam. Additionally, there are two minima at about 706 and 718 eV, corresponding to the L_3 and L_2 absorption edges of iron. When an external magnetic field of about $H = 3000$ Oe is applied perpendicular to the direction of the scattering vector and in the plane of incidence, the intensities of the minima differ for right (+) or left (−) circularly polarized radiation. In Figure 2, the difference in reflectance is displayed by the asymmetry ratio $A(E) = (I_+ - I_-)/(I_+ + I_-)$. The nonzero asymmetry ratio at both absorption edges is clear evidence of the magnetization of the sample, which is supported by the control experiment which showed that no dichroic signal is observed without applied field. Generally, the refractive index $n = 1 - (\delta \pm \Delta\delta) + i(\beta \pm \Delta\beta)$ is a complex quantity, and both real (dispersion δ) and imaginary parts (proportional to absorption) depend on the electron density and the contributions ($\Delta\delta$, $\Delta\beta$) from the magnetic moment of the material.[31] Usually, XMCD is measured in transmission geometry where the absorption term dominates the experiment. This is not the case for the present experiment because in reflection geometry both terms ($\Delta\delta$, $\Delta\beta$) contribute to the signal. To interpret the data, we use ab initio calculations to determine the energy-dependent contribution of $\Delta\delta$(E) and $\Delta\beta$(E) to the reflectance.[32] These values are used to determine the complex refractive index, which in turn serves to compute the energy-dependent reflectance with the Fresnel equations. Applying sum rules to the absorption part $\beta \pm \Delta\beta$ of the complex refractive index, n, we obtain a magnetic moment of $0.5 \pm 0.3\ \mu_B$ per iron ion for the spin momentum and $0.01 \pm 0.01\ \mu_B$ per iron ion for the orbit momentum. These values are in good agreement with the neutron measurements (vide supra).

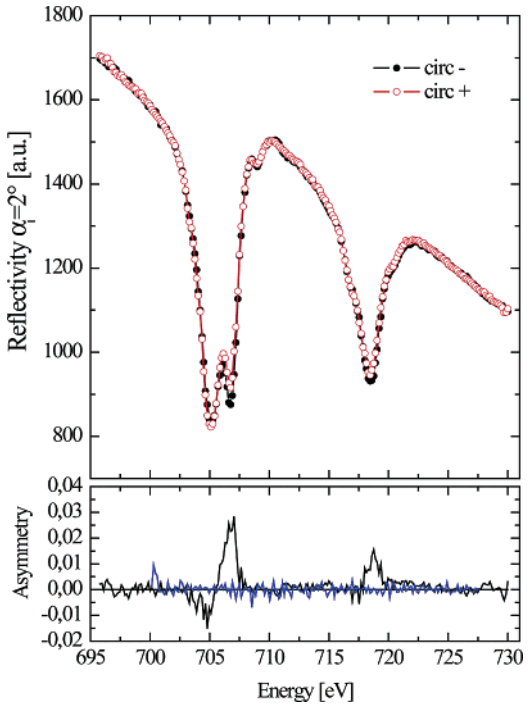

Figure 2. (Top) X-ray magnetic circular dichroism (XMCD) measurements at the $L_{3,2}$ edge of iron of an 11-monolayer sample. (Bottom) The asymmetry ratio $A(E) = (I_+ - I_-)/(I_+ + I_-)$ between left and right circularly polarized light demonstrates the occurrence of molecular magnetism. The blue line indicates $A(E)$ without an applied magnetic field.

In conclusion, we propose that a phase transition in an amphiphilic mesophase can induce sufficient (mechanical) strain to distort the coordination sphere of the tightly coupled Fe(II) centers in MEPE. The distortion is strong enough to reduce the strength of the ligand field, giving rise to spin transition from low to high spin state. The observed high-temperature molecular magnetism differs from those of other magnetic materials. Instead of competing spin ordering versus thermal disorder, the present material is characterized by spin transition induced by gap reduction. Liquid crystalline materials are readily processed

(32) Kune, J.; Oppeneer, P. M.; Mertins, H.-Ch.; Schäfers, F.; Gaupp, A.; Gudat, W.; Novak, P. *J. Magn. Magn. Mater.* **2002**, *240*, 454−456.
(33) Meister, A.; Förster, G.; Thünemann, A.; Kurth, D. G. *ChemPhysChem* **2003**, *4*, 1095−1100. Kurth, D. G.; Severin, N.; Rabe, J. P. *Angew. Chem.* **2002**, *41*, 3833−3835; *Angew. Chem., Int. Ed.* **2002**, *114*, 3681−3683.

into various device architectures, and the concept can be extended to virtually all metallo-supramolecular polymers with suitable electronic configurations, giving access to a plethora of new materials.[33]

Acknowledgment. The authors thank Prof. Westerholt for experimental support. This work is funded by the DFG Schwerpunktprogramm "Molekularer Magnetismus" (SPP 1137).

Note Added after ASAP Publication: In the version published on the Internet February 10, 2005, there was a production error in the y-axis label for Figure 2. In the final version published February 17, 2005, and the print version Figure 2 is correct.

JA0447210